Wireless Detection of Trace Ammonia: A **Chronic Kidney Disease Biomarker**

Shao-Xiong Lennon Luo and Timothy M. Swager*

Cite This: ACS Nano 2024, 18, 364-372



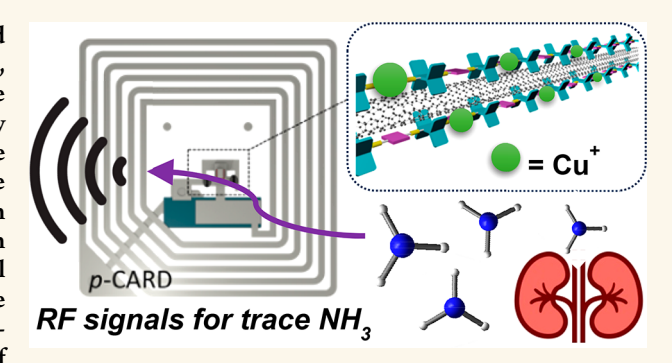
ACCESS

Metrics & More

Article Recommendations

Supporting Information

ABSTRACT: Elevated levels of ammonia in breath can be linked to medical complications, such as chronic kidney disease (CKD), that disturb the urea balance in the body. However, early stage CKD is usually asymptomatic, and mass screening is hindered by high instrumentation and operation requirements and accessible and reliable detection methods for CKD biomarkers, such as trace ammonia in breath. Enabling methods would have significance in population screening for early stage CKD patients. We herein report a method to effectively immobilize transition metal selectors in close proximity to a single-walled carbon nanotube (SWCNT) surface using pentiptycene polymers containing metalchelating backbone structures. The robust and modular nature of



the pentiptycene metallopolymer/SWCNT complexes creates a platform that accelerates sensor discovery and optimization. Using these methods, we have identified sensitive, selective, and robust copper-based chemiresistive ammonia sensors that display low parts per billion detection limits. We have added these hybrid materials to the resonant radio frequency circuits of commercial near-field communication (NFC) tags to achieve robust wireless detection of ammonia at physiologically relevant levels. The integrated devices offer a noninvasive and cost-effective approach for early detection and monitoring of CKD.

KEYWORDS: ammonia sensing, chronic kidney disease, carbon nanotubes, conjugated polymers, wireless sensing

INTRODUCTION

Downloaded via MASSACHUSETTS INST OF TECHNOLOGY on February 12, 2024 at 15:50:45 (UTC) See https://pubs.acs.org/sharingguidelines for options on how to legitimately share published articles.

Chronic kidney disease (CKD) is a common chronic disease estimated to affect more than 10% of the population in many regions of the world. 1-6 Early detection of CKD is essential as it allows room for early interventions and therapies to slow down the disease progression.^{2,7} CKD at early stages is usually asymptomatic, and as a result of a lack of population screening programs, most patients with CKD are unaware of their condition until they reach later stages with poor prognosis.^{8,9} For patients diagnosed with late-stage CKD, constant and prompt monitoring is critical to evaluate the need for dialysis.² However, conventional methods to diagnose and monitor CKD are based on blood and urine tests that are laborintensive and time-consuming, 1,10 thereby creating a barrier to routine testing and hindering timely interventions. Therefore, it is imperative to develop an accessible diagnostic tool for rapid screening and easy monitoring of CKD, which can significantly improve the quality of life for the patients.

CKD is characterized by the loss of kidney function to filter metabolic waste, 1,2 which causes an accumulation of waste in the circulatory system with an elevated ammonia level in blood, breath, and bodily fluids. As a result, ammonia is a valuable biomarker for the screening and monitoring of CKD. 11-14 The breath ammonia levels in healthy individuals

are generally in the low parts per billion (ppb) concentrations. 15 However, the breath ammonia levels of late-stage CKD patients are significantly higher and can reach 10 parts per million (ppm). 11 Although a breath ammonia test may not replace standard blood and urine tests, it can serve as a complementary tool to rapidly screen asymptomatic patients and provide home-based noninvasive real-time monitoring for CKD patients. Moreover, an accessible and robust ammonia detection method carries additional merits, as elevated ammonia levels are also linked to other medical conditions such as *H. pylori* infection that produces ammonia in the stomach 16-18 or genetic disorders such as ornithine transcarbamylase deficiency (OTCD) that hinders ammonia metabolism. 19-21

Existing methods for trace ammonia detection include gas chromatography,²² ion mobility spectrometry,^{23,24} photoacoustic spectroscopy,²⁵ and fluorescence spectroscopy.²⁶

Received: August 6, 2023 Revised: December 19, 2023 Accepted: December 21, 2023 Published: December 26, 2023





These methods have high accuracy yet require expensive instrumentation, making them less ideal as point-of-care tests for CKD patients, especially in less developed regions of the world.²⁷ Alternatively, chemiresistive sensors that transduce chemical interactions to electrical readouts, have become increasingly popular due to their simple fabrication and high sensitivity, making them suitable for the continuous monitoring of target analytes. ^{28–33} Among the different chemiresistive materials used, single-walled carbon nanotubes (SWCNTs) have attracted increasing attention because they operate at ambient temperature, have tunable selectivity, display small form factors, are rapidly prototyped, with low cost, high scalability, and adaptability for integration into portable electronic devices. 32-38 These advantages of SWCNTs, especially the miniature size and low cost and power requirements, make them appealing as the sensing materials for the envisioned home-based diagnostic tool for CKD.

By leveraging the electron-donating properties of ammonia, we targeted SWCNTs adorned with electrophilic metal complexes that serve as selectors. The goal is to enhance the effective charge transfer from ammonia to the p-doped SWCNTs and thereby modulating the conductance.³² To enhance this chemiresistive response in metal-functionalized SWCNTs, it is essential to construct a robust interface with strong electronic coupling between metal complexes and SWCNTs. We have previously shown that pentiptycene-based conjugated polymers, such as P4 in Figure 1a, effectively bind and disperse small diameter SWCNTs in organic solvents and significantly improve their sensing performance. 39,40 To expand the functionalities of these SWCNT binding polymers to include transition metals, we have introduced metal chelation sites in the backbone (Figure 1a). Contrary to other polymer-wrapped SWCNTs, where metal species are anchored by pendant functional groups that are not necessarily in direct communication with the SWCNTs, 41-43 the metal species chelated to the backbone of these pentiptycene polymers are positioned to interact directly with the graphene sidewalls of SWCNTs (Figure 1b). Therefore, any electronic changes at the metal centers are expected to result in greater charge transfer (doping) effects and provide higher chemiresistive responses. This functionalization scheme is noncovalent and preserves the semiconducting properties of SWCNTs that are critical to chemiresistive sensing.⁴⁴ The rigid pentiptycene units in these polymers also produce internal free volume to create porous interstitial cavities. These iptycene-based porous nanostructures are conducive to gas analyte diffusion and have shown to facilitate the analyteselector interactions in gas sensing. 39,40,42 The solution processability of the resulting pentiptycene polymer/SWCNT complexes also provides a practical and scalable sensor fabrication. More importantly, this modular platform enables rapid sensor screening to identify the optimal transition-metalbased selectors for sensors of specific needs.

In this study, we utilize pentiptycene metallopolymer/SWCNT complexes to create sensitive, selective, and robust sensors for the detection of trace ammonia at levels relevant to utility as a biomarker for chronic kidney disease. Incorporating the sensors into accessible near-field communication (NFC) tags, we have developed a wireless detection system for ammonia testing at physiologically relevant levels and thereby demonstrate a noninvasive cost-effective approach for early detection and monitoring of chronic kidney disease.

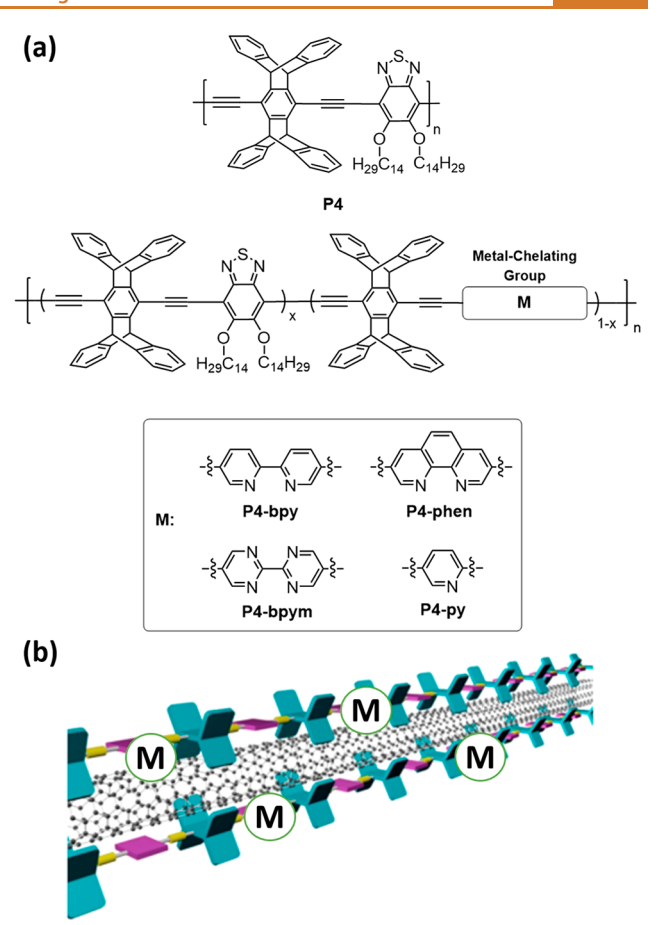


Figure 1. (a) Structural drawings of pentiptycene-based polymers. (b) Schematic drawing of pentiptycene metallopolymer/SWCNT complex. (bottom) Adapted from ref 39. Copyright 2020 American Chemical Society.

RESULTS AND DISCUSSION

We synthesized a series of pentiptycene-based metal-chelating polymers by a statistical Sonogashira coupling copolymerization using 6,13-diethynylpentiptycene and equimolar amounts of 4,7-dibromo-5,6-bis(tetradecyloxy)benzo-2,1,3-thiadiazole and comonomers containing metal chelating bipyridine, phenanthroline, bipyrimidine, and pyridine moieties (Figure S1). The successful copolymerization is revealed by gel permeation chromatography (GPC), ¹H NMR, as well as high-resolution X-ray photoelectron spectroscopy (XPS), wherein the atomic ratios between nitrogen and sulfur species were found to agree with the theoretical compositions of the copolymers (Table S1, Figures S2-S6). Following our previously reported procedures, 39 we prepared pentiptycene polymer/SWCNT dispersions by sonicating the components in ortho-dichlorobenzene (oDCB). Centrifugation removes the large SWCNT aggregates and amorphous carbon impurities, yielding homogeneous stable dispersions. Consistent with the previous study,³⁹ the noncovalent functionalization of SWCNTs using pentiptycene polymers does not result in significant disruption to the CNT surface π -conjugation as indicated by the absence of an enhanced Raman defect band (D-band) at ~1300 cm⁻¹ (Figure S7).^{45,46} Taking advantage of the high processability of these pentiptycene polymer/ SWCNT dispersions, we fabricated chemiresistive devices simply by drop-casting a small amount of the dispersion (1 μ L) between gold electrodes deposited on a glass substrate. The

subsequent metal coimmobilization was achieved by submerging the devices in DMF solutions of metal salts for 12 h. For example, the successful chelation of CuOTf (OTf = CF₃SO₃⁻) by the pentiptycene polymers is evidenced by the formation of an XPS N 1s peak with significantly higher binding energy that can be assigned to pyridinic nitrogen chelated to metal species (Figure S8a). 47-49 XPS analysis also suggests the formation of Cu²⁺ species with characteristic Cu 2p satellite peaks,⁵⁰ possibly due to aerobic oxidation (Figure S8b). With the fabricated devices at hand, we then tested their chemiresistive response to trace ammonia in dry air, which is evaluated as the normalized changes in their resistance (ΔR / R_0 , where ΔR is the change in resistance and R_0 represents the baseline resistance). A typical testing procedure includes setting the devices under constant airflow for 30 min to establish a baseline, followed by a 5 min exposure to ammonia at controlled concentration levels, and then a recovery period in analyte-free carrier gas. Minor linear baseline corrections are used to address linear baseline resistance drift.³³ As a result of the simple fabrication and derivatization of chemiresistive devices made from the pentiptycene polymer/SWCNT complexes, we could perform quick sensor screening with a variety of transition metal species, including Cu⁺, Co²⁺, Fe³⁺, Ir³⁺, Ni²⁺, Pt²⁺, Rh³⁺, and Ru³⁺. As shown in Figure S9, using P4-bpy as the model polymer substrate, we identified CuOTf as the best performer with the highest chemiresistive response toward 100 ppm ammonia (211.5%). The sensing traces of devices made of P4-bpy/CuOTf showed large, quick, and reversible chemiresistive changes with low device-to-device variability (Figure 2). In the control experiments where we

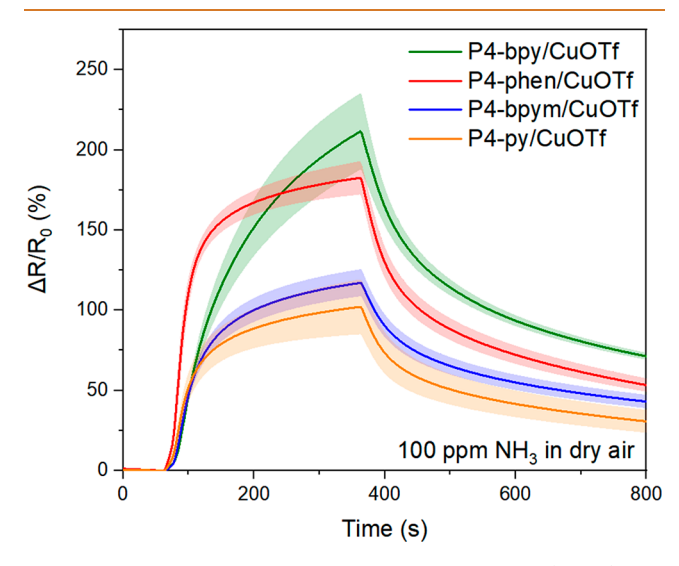


Figure 2. Chemiresistive responses of P4-bpy/CuOTf (green), P4-phen/CuOTf (red), P4-bpym/CuOTf (blue), and P4-py/CuOTf (orange) to ammonia. Devices were exposed to 100 ppm ammonia in dry air for 5 min. $(N \ge 4)$.

removed CuOTf (P4-bpy-SWCNT) and the pentiptycene polymer (pSWCNT/CuOTf), we observed significantly lower responses (Figure S10). The elevated ammonia sensitivity of P4-bpy/CuOTf could be attributed to the synergistic effect of the high affinity between the electron-donating ammonia and the copper center as well as the strong electronic coupling provided by the bipyridine ligands. It is also worth highlighting that there is an apparent positive correlation between the density of the metal-chelating groups on the polymer backbone

and the chemiresistive response toward ammonia. We compared the performance of the devices containing 50% (P4-bpy/CuOTf), 20% (P4-bpy20/CuOTf), and 0% (P4/CuOTf) bipyridine groups (Figure S10). Moreover, P4-bpy/CuOTf displayed much higher responses than devices made from a commercial bipyridine-containing polyfluorene that has been widely used in dispersing and sorting SWCNTs (PFO-bpy/CuOTf). S1-53

The choice of the metal-chelating group in the polymer also seems to influence the chemiresistive response to ammonia. As shown in Figure 2, we compared the responses to 100 ppm ammonia in sensors made from the series of pentiptycene polymers bearing different metal chelating comonomers. Although sensors with phenanthroline moieties (P4-phen/ CuOTf) were found to possess similar sensitivity to ammonia as sensors made from a bipyridine-containing polymer (P4bpy/CuOTf), sensors with the monodentate pyridine groups (P4-py/CuOTf) or the electronically distinct bipyrimidine groups (P4-bpym/CuOTf) displayed significantly lower sensitivities. These demonstrate that the sensor performance can be effectively modulated by molecular engineering of the polymer backbone. Moreover, these results suggest the potential in these structurally diverse pentiptycene metallopolymer/SWCNT complexes in sensor arrays that can generate distinct response profiles to achieve analyte identification and classification within complex environments.54-56

Although pristine CNTs possess some degree of intrinsic sensitivity to ammonia, ^{57,58} we attribute the mechanism for the enhanced ammonia responses in our sensors to the interactions with the immobilized copper centers. The electronic coupling between the metals and the graphene sidewalls results in a decreased carrier concentration or carrier pinning upon exposure to ammonia, inducing an increase in the resistivity of SWCNTs. An *n*-type (dedoping) response is consistent with previous ammonia sensing systems employing transition metal species as selectors on SWCNTs. 59-61 To rule out the reduction/oxidation sensing mechanism, where the metal center is formally reduced by ammonia, we performed the sensing test under a nitrogen environment, and no significant difference was observed in sensor sensitivity or reversibility (Figure S11), supporting the chemisorption/ desorption mechanism without parallel redox complications.

To characterize the sensitivity of our sensors, we evaluated the chemiresistive responses of P4-bpy/CuOTf in different levels of ammonia in dry air. As shown in Figure 3b, we observed an increasing chemiresistive response of P4-bpy/CuOTf as a function of the ammonia concentration. More importantly, we observed significant chemiresistive responses to ammonia at physiologically relevant concentrations (Figure 3c). The chemiresistive responses to ammonia also possess a linear relationship with ammonia concentrations (Figure 3d) so that the ammonia level can be quantified with high confidence. The average limit of detection (LOD) of the P4-bpy/CuOTf chemiresistive ammonia sensor is calculated to be 57 ppb, placing it in the same league among the most sensitive room-temperature chemiresistive ammonia sensors reported (Table S2).

Besides meeting the requirement in sensor sensitivity to detect trace levels of ammonia, the sensor also needs to be selective when challenged with common interfering agents found in breath. As shown in Figure 4, P4-bpy/CuOTf displays superior selectivity toward ammonia against a series of

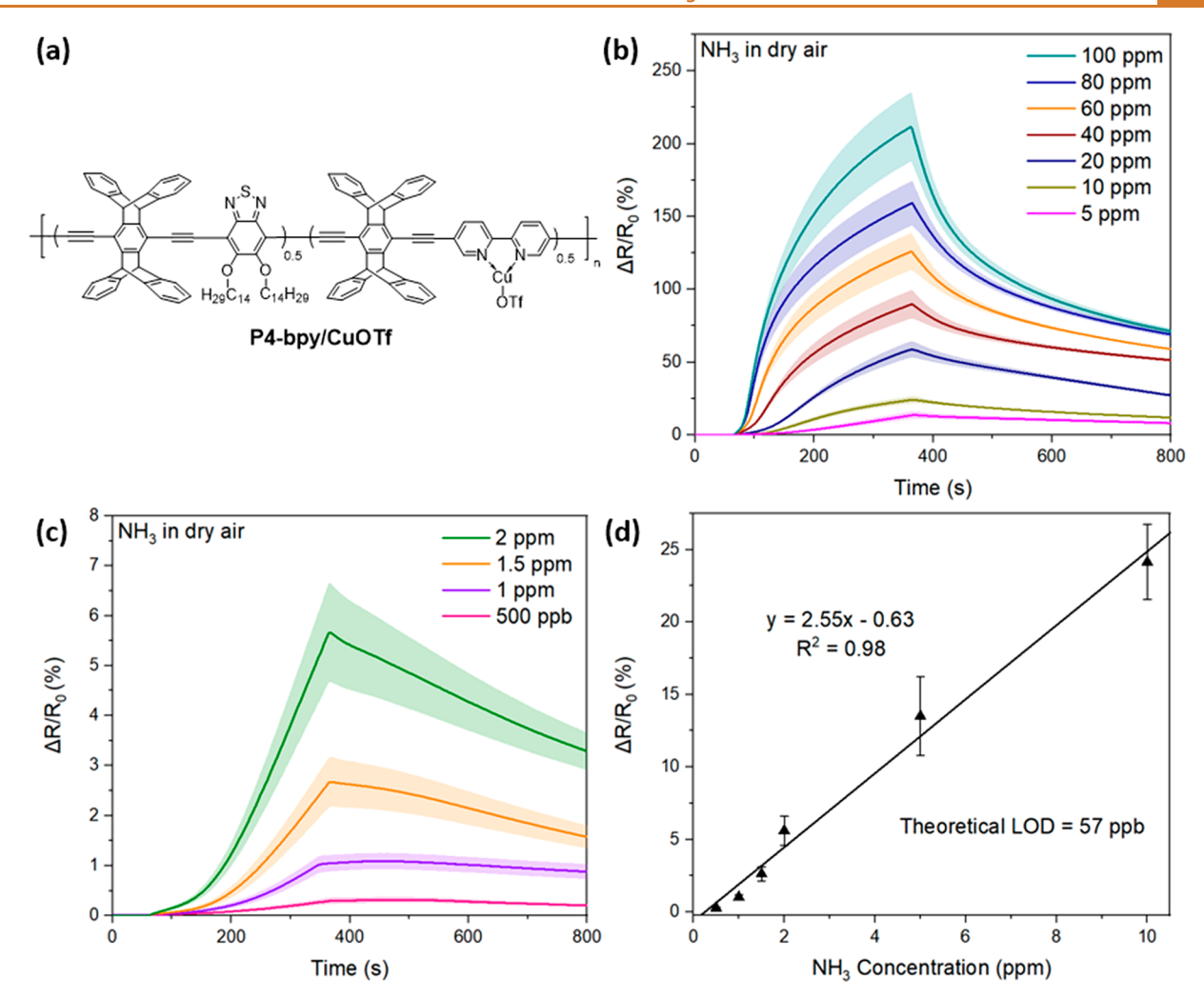


Figure 3. (a) Polymer structure of P4-bpy/CuOTf. (b) Chemiresistive responses of P4-bpy/CuOTf to ammonia (5 ppm-100 ppm) in dry air for 5 min. (c) Chemiresistive responses of P4-bpy/CuOTf to ammonia (500 ppb-2 ppm) in dry air for 5 min. (d) Calibration curve of P4-bpy/CuOTf to ammonia (500 ppb-10 ppm) in dry air for 5 min. ($N \ge 4$).

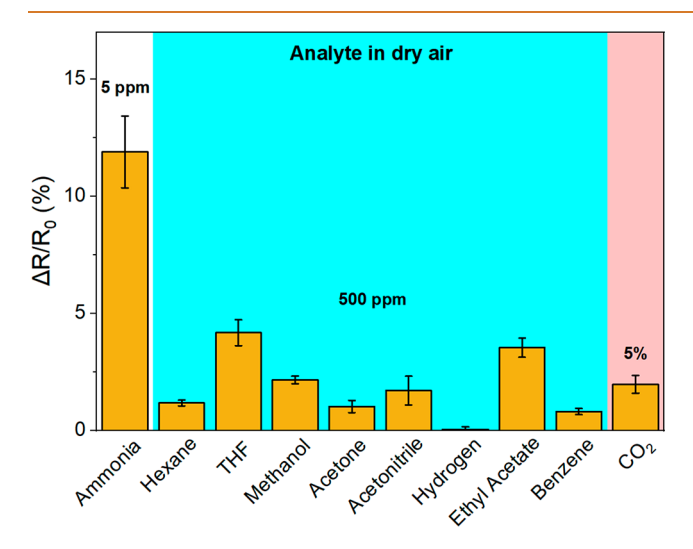


Figure 4. Chemiresistive responses of P4-bpy/CuOTf toward volatile organic compounds and gases in dry air for 5 min. $(N \ge 4)$.

gases and volatile organic compounds, even when the ammonia concentration is 2 to 4 orders of magnitude lower than the interferants. Moreover, P4-bpy/CuOTf displays insignificant

responses toward trace H_2S (Figure S12), which is often present in exhaled breath.^{65,66}

Another critical requirement for a functional sensor for breath analysis is the tolerance to high humidity as the exhaled breath typically contains saturated moisture. Drying columns have been employed in breathalyzers to mitigate the humidity effect, albeit at the expense of an increased instrumentation cost.⁶⁷ Hence a sensor with intrinsic tolerance to humidity is necessary for practical breath analysis. As shown in Figure 5 and Figure S13, in high humidity levels (>60% relative humidity), the chemiresistive responses of P4-bpy/CuOTf to 10 ppm ammonia are minimally impacted. This humidity tolerance is significant when it is considered that excess water can competitively bind to the selector, highlighting the notable selectivity of P4-bpy/CuOTf to ammonia. Although the humidity effect is more prominent when the ammonia concentration is at 100 ppm (Figure 5, Figure S14), this ammonia concentration is much higher than the physiologically relevant level. We note that differences with humidity may also be related to the observed increases in the baseline resistance (Figure S15).⁶⁸⁻⁷⁰ This may be indicative of an initial depletion of mobile hole carriers that are capable of being modulated by n-type dopant ammonia. The fast saturation of the chemiresistive responses to high concen-

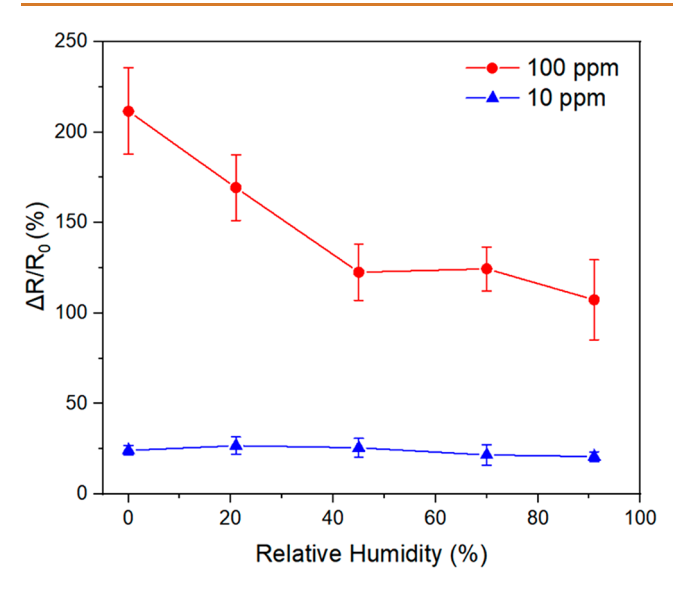


Figure 5. Summary of chemiresistive responses of P4-bpy/CuOTf to 100 ppm of ammonia (red) and 10 ppm of ammonia (blue) with respect to relative humidity. $(N \ge 4)$.

trations of ammonia is consistent with this possibility (Figure S14). We also observed an increased sensor recovery kinetics under high humidity (Figure S13, Figure S14), consistent with a previous report of water-assisted desorption of ammonia from SWCNTs.⁷⁰

P4-bpy/CuOTf exhibits good reusability and long-term stability under ambient storage conditions. The chemiresistive responses are retained after repeated ammonia exposure (Figure S16) and month-long aging (Figure S17), highlighting the robustness of the device.

To make an accessible home-based diagnostic tool, we have incorporated **P4-bpy/CuOTf** chemiresistive sensors into smartphone readable NFC tags $^{43,71-73}$ for noninvasive and real-time monitoring of ammonia levels. For this application, CuOTf is added to the **P4-bpy** SWCNT dispersion. We then drop-cast the metalated dispersion on an inexpensive commercial NFC tag to introduce a parallel circuit within the existing circuit of the NFC tag to fabricate a parallel-chemically actuated resonant device (p-CARD) (Figure 6).

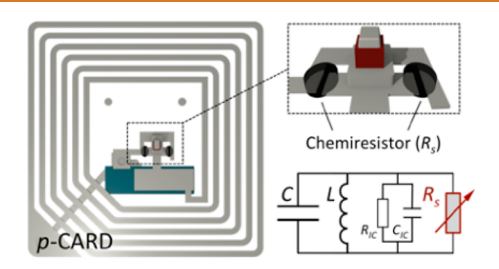


Figure 6. Schematic design of *p*-CARD, showing the location for the drop-cast and the modified circuit design incorporating the chemiresistor. Adapted from ref 43. Copyright 2017 American Chemical Society.

The change in the resistance of the chemiresistor results in a change in the gain amplitude of the p-CARD at the resonant frequency, $^{71-73}$ due to the change in the efficiency of energy transfer between the tag and the reader. The fabricated p-CARDs are placed in a sensing chamber under constant airflow and measured by a vector network analyzer (VNA) with a

copper antenna positioned at a fixed distance over a 10-20 MHz frequency range. A typical wireless sensor testing workflow includes 30 min of constant airflow to establish the baseline, 15 min of ammonia exposure, and 1 h of recovery under air. The sensor response is defined by the difference in the gain amplitude before and after ammonia exposure ($\Delta Gain$, dB).

Control experiments using unmodified NFC tags and metalfree P4-bpy/SWCNT complexes showed insignificant responses to ammonia (Figure S18). Gain responses of a representative p-CARD containing P4-bpy/CuOTf are shown in Figure 7a. A significant change in gain amplitude at the resonant frequency (0.5 dB) was observed when the P4-bpy/ **CuOTf** *p*-CARD was exposed to 100 ppm ammonia in dry air. To determine the speed of ammonia response of the P4-bpy/ CuOTf p-CARDs, we have evaluated the p-CARD responses with respect to the duration of ammonia exposure. As shown in Figure S19, most of the responses took place within the first few minutes of ammonia exposure, whereas maximum responses were reached within 15 min. Trace ammonia (2 ppm) can also be detected with a significant change in gain amplitude at the resonant frequency (0.06 dB), owing to the robust baseline. Duplicate devices showed similar responses to ammonia in dry air (Figure S20). The P4-bpy/CuOTf p-CARDs also display excellent reversibility (Figure S20). Moreover, we can establish a calibration curve with high confidence with exponential fitting between p-CARD responses and ammonia concentrations where trace levels of ammonia can be effectively quantified. As gain amplitudes are expressed in decibels, this logarithmic relationship between gain amplitudes and ammonia concentrations is consistent with the linear dependency shown in the chemiresistive measurements (Figure 3),⁷² suggesting similar operative sensing mechanisms in the two types of approaches. The average calculated LOD is 130 ppb for these devices. More importantly, the ammonia responses of P4-bpy/CuOTf p-CARDs were mostly retained in high humidity (Figure S21). These results highlight the potential utility of p-CARDs consisting of pentiptycene metallopolymer/SWCNT complexes in serving as an accessible, noninvasive, and practical platform for the rapid screening and easy monitoring of CKD.

CONCLUSION

In pursuit of sensitive and selective chemiresistive sensors for ammonia, we have reported a method to effectively immobilize transition metal selectors on SWCNT-based chemiresistors using pentiptycene polymers containing metal-chelating backbone structures. These molecularly tunable metal-chelating pentiptycene polymer/SWCNT complexes serve as a modular platform for rapid sensor screening. As a result, we have identified Cu-chelated pentiptycene polymer/SWCNT complexes as selective, sensitive, and robust chemiresistive sensors for detecting trace ammonia at levels wherein it can serve as a breath biomarker for chronic kidney disease. Furthermore, the sensors can be integrated into accessible NFC tags to enable the wireless detection of ammonia at physiologically relevant concentrations. These sensors offer a noninvasive and costeffective approach for early detection and easy monitoring of CKD, which can improve the quality of life for patients.

MATERIALS AND METHODS

Materials. Commercial reagents were purchased from Sigma-Aldrich, Alfa Aesar, Combi-Blocks, Oakwood, and Ambeed Inc. and

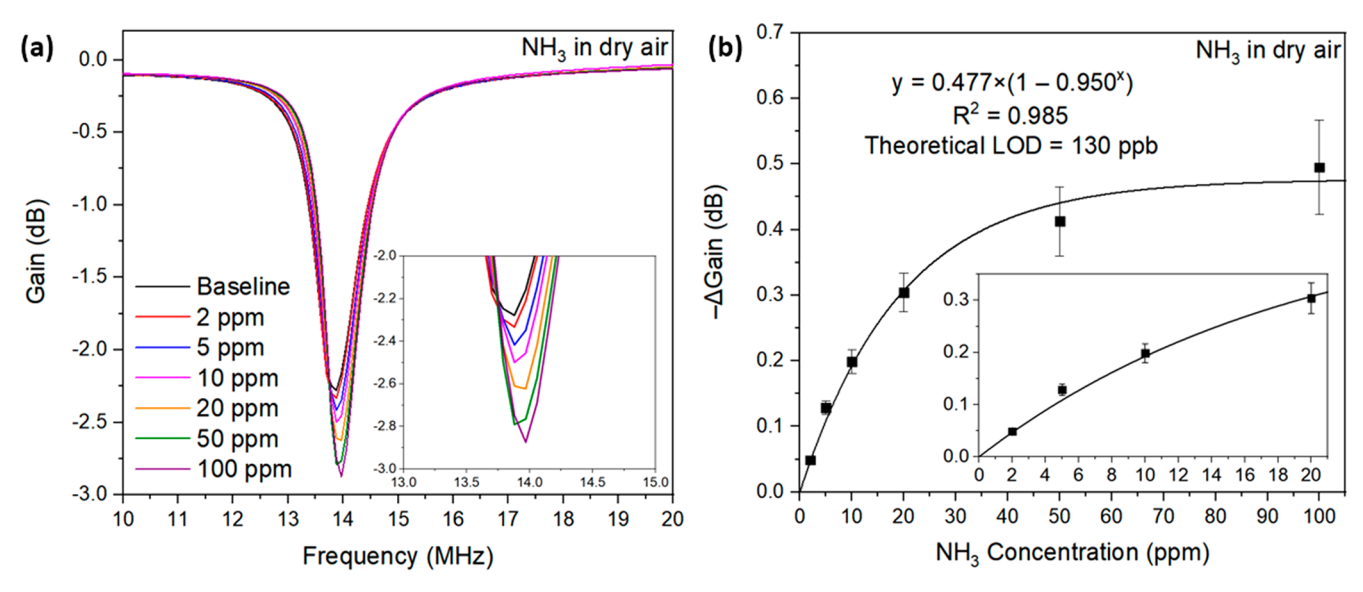


Figure 7. Wireless detection of ammonia by P4-bpy/CuOTf p-CARDs. (a) Resonance-frequency traces of a representative P4-bpy/CuOTf p-CARD in response to different concentrations of ammonia in dry air for 15 min. (b) Correlation of magnitude of response (Δ Gain) at the resonant frequency and ammonia concentrations. (N = 3).

used as received unless otherwise noted. Deuterated solvents were purchased from Cambridge Isotope Laboratories and used as received. Single-walled carbon nanotubes [Signis SG65i, lot no.: MKBZ1159V; (6,5) chirality, \geq 93% carbon as SWCNT; 0.7–0.9 nm diameter) were purchased from Sigma-Aldrich and used as received. **PFO-bpy** (Poly[(9,9-dioctylfluorenyl-2,7-diyl)-alt-co-(6,6'-(2,2'-bi-pyridine))], ADS153UV, $M_{\rm n}=134$ kDa, lot no. 21H003A1) was purchased from American Dye Source Inc. and used as received. Gas cylinders were purchased from Airgas. 6,13-Diethynylpentiptycene, 75 4,7-dibromo-5,6-bis(tetradecyloxy)benzo-2,1,3-thiadiazole, and P4⁷⁷ were synthesized according to procedures in literature.

Instrument. NMR spectra were recorded by using a Bruker Avance 500 MHz NMR spectrometer. Polymer samples were analyzed in THF using an Agilent 1260 Infinity GPC system with variable wavelength diode array (254, 450, and 530 nm) and refractive index detectors. The instrument was calibrated with narrow-dispersity polystyrene standards between 1.7 and 3150 kg mol⁻¹. Tip sonication was performed with a Qsonica Q125 sonicator. Bath sonication was performed with a Branson B5510 sonicator. Raman spectra were collected using a Horiba Jobin-Yvon LabRam (Model HR 800) Raman confocal microscope with a 633 nm laser. X-ray photoelectron spectroscopy (XPS) measurements were performed on a Thermo Scientific K-Alpha+ X-ray photoelectron spectrometer. Mass flow controllers (MFCs) were purchased from Alicat Scientific, with carrier gas flow rates (air or nitrogen) controlled using an MC-10SLPM-D/ 5M and analyte gas flow rates controlled using an MC-10SCCM-D/ 5M. Analyte gases from volatile organic compounds were generated by a FlexStream FlexBase module. Device resistance was measured using an Agilent Keysight 34970A data logger equipped with a 34901A 20-channel multiplexer module. Commercial RFID tags were used (Texas Instruments, HF-I Tag-It Plus Transponder Inlays, and TI-Tag) and were converted to resonant devices for wireless chemical sensing. The RFID tags were used as received, and the RF signals were monitored from 10 to 20 MHz using a copper loop probe as antenna that was connected to an Agilent E5061B network analyzer.

Synthesis of P4-bpy. 6,13-Diethynylpentiptycene (0.20 mmol), 4,7-dibromo-5,6-bis(tetradecyloxy)benzo-2,1,3-thiadiazole (0.10 mmol), 5,5'-dibromo-2,2'-bipyridine (0.10 mmol), tetrakis(triphenylphosphine)palladium(0) (0.01 mmol), and copper(I) iodide (0.02 mmol) were placed in a Schlenk flask equipped with a magnetic stirrer. Contents were evacuated and backfilled with argon 5 times. Degassed toluene (3 mL) and diisopropylamine (1 mL) were added to the flask, and after 5 more freeze—pump—thaw cycles with liquid nitrogen, the resulting mixture was stirred at room temperature

for 30 min followed by 48 h at 65 C and 24 h at 75 C. After cooling to room temperature, contents were precipitated in methanol, isolated by filtration with nylon membrane filter, and washed with methanol. The resulting polymer was washed with hot acetone for 6 h and extracted with hot chloroform using a Soxhlet apparatus and dried under reduced pressure. GPC (THF vs PS): $Mn = 3.5 \times 10^4$ Da, PDI = 1.8.

Synthesis of P4-phen. 6,13-Diethynylpentiptycene (0.20 mmol), 4,7-dibromo-5,6-bis(tetradecyloxy)benzo-2,1,3-thiadiazole (0.10 mmol), 3,8-dibromo-1,10-phenanthroline (0.10 mmol), tetrakis(triphenylphosphine)palladium(0) (0.01 mmol), and copper(I) iodide (0.02 mmol) were placed in a Schlenk flask equipped with a magnetic stirrer. Contents were evacuated and backfilled with argon 5 times. Degassed anisole (3 mL) and diisopropylamine (1 mL) were added to the flask, and after 5 more freeze—pump—thaw cycles with liquid nitrogen, the resulting mixture was stirred at room temperature for 30 min followed by 48 h at 150 C. After cooling to room temperature, contents were precipitated in methanol, isolated by filtration with nylon membrane filter, and washed with methanol. The resulting polymer was washed with hot acetone for 6 h and extracted with hot chloroform using Soxhlet apparatus and dried under reduced pressure. GPC (THF vs PS): $Mn = 1.4 \times 10^4$ Da, PDI = 1.9.

Synthesis of P4-bpym. 6,13-Diethynylpentiptycene (0.20 mmol), 4,7-dibromo-5,6-bis(tetradecyloxy)benzo-2,1,3-thiadiazole (0.10 mmol), 5,5'-dibromo-2,2'-bipyrimidine (0.10 mmol), tetrakis(triphenylphosphine)palladium(0) (0.01 mmol), and copper(I) iodide (0.02 mmol) were placed in a Schlenk flask equipped with a magnetic stirrer. Contents were evacuated and backfilled with argon 5 times. Degassed anisole (3 mL) and diisopropylamine (1 mL) were added to the flask, and after 5 more freeze—pump—thaw cycles with liquid nitrogen, the resulting mixture was stirred at room temperature for 30 min followed by 48 h at 150 °C. After cooling to room temperature, contents were precipitated in methanol, isolated by filtration with nylon membrane filter, and washed with methanol. The resulting polymer was washed with hot acetone for 6 h and extracted with hot chloroform using Soxhlet apparatus and dried under reduced pressure. GPC (THF vs PS): $Mn = 1.5 \times 10^4$ Da, PDI = 2.2.

Synthesis of P4-py. 6,13-Diethynylpentiptycene (0.20 mmol), 4,7-dibromo-5,6-bis(tetradecyloxy)benzo-2,1,3-thiadiazole (0.10 mmol), 2,5-dibromopyridine (0.10 mmol), tetrakis-(triphenylphosphine)palladium(0) (0.01 mmol), and copper(I) iodide (0.02 mmol) were placed in a Schlenk flask equipped with a magnetic stirrer. Contents were evacuated and backfilled with argon 5 times. Degassed toluene (3 mL) and diisopropylamine (1 mL) were

added to the flask, and after 5 more freeze–pump—thaw cycles with liquid nitrogen, the resulting mixture was stirred at room temperature for 30 min followed by 48 h at 65 °C and 24 h at 75 °C. After cooling to room temperature, contents were precipitated in methanol, isolated by filtration with nylon membrane filter, and washed with methanol. The resulting polymer was washed with hot acetone for 6 h and extracted with hot chloroform using Soxhlet apparatus and dried under reduced pressure. GPC (THF vs PS): $Mn = 3.8 \times 10^4$ Da, PDI = 2.1.

Synthesis of P4-bpy20. 6,13-Diethynylpentiptycene (0.20 mmol), 4,7-dibromo-5,6-bis(tetradecyloxy)benzo-2,1,3-thiadiazole (0.16 mmol), 5,5'-dibromo-2,2'-bipyridine (0.04 mmol), tetrakis(triphenylphosphine)palladium(0) (0.01 mmol), and copper(I) iodide (0.02 mmol) were placed in a Schlenk flask equipped with a magnetic stirrer. Contents were evacuated and backfilled with argon 5 times. Degassed toluene (3 mL) and diisopropylamine (1 mL) were added to the flask, and after 5 more freeze–pump—thaw cycles with liquid nitrogen, the resulting mixture was stirred at room temperature for 30 min followed by 48 h at 65 °C and 24 h at 75 °C. After cooling to room temperature, contents were precipitated in methanol, isolated by filtration with nylon membrane filter, and washed with methanol. The resulting polymer was washed with hot acetone for 6 h and extracted with hot chloroform using Soxhlet apparatus and dried under reduced pressure. GPC (THF vs PS): $Mn = 4.6 \times 10^4$ Da, PDI = 1.9.

Preparation of SWCNT Dispersion. For pristine SG65i SWCNTs, a stock solution of SG65i SWCNTs (2 mg) was prepared in o-dichlorobenzene (oDCB) (20 mL) by bath sonication at RT for 30 min. Subsequently, the suspension was allowed to stand overnight undisturbed. For polymer/SWCNT dispersions, polymer (2 mg) was dissolved in o-dichlorobenzene (oDCB, 2 mL), and the solution was sonicated in a water bath for 10 min. To the polymer solution was added 0.2 mg of SG65i SWCNTs, and the resulting mixture was chilled with ice and homogenized for 20 min using a Qsonica Q125 sonicator at 63W with a pulse sequence (10 s ON and 5 s OFF). Subsequently, the suspension was centrifuged for 3 h at 22000g. The top 80% of the supernatant was isolated and used.

Chemiresistive Device Preparation. Glass slides (VWR microscope slides) were cleaned with oxygen plasma for 15 min (Harrick PDC-32G Plasma Cleaner), bath sonicated in acetone for 15 min, and then dried with a stream of nitrogen. Using an aluminum mask, chromium (15 nm) followed by gold (50 nm) was deposited using a Thermal Evaporator (Angstrom Engineering), leaving a 0.5 mm gap between the gold electrodes. A 1 μ L amount of the SWCNT dispersion was drop-casted in between the gold electrodes and dried at RT under house vacuum in a desiccator or vacuum oven. Subsequently, the glass slides were submerged in a solution of metal salt (10 mg/mL) in N_iN -dimethylformamide (DMF) in a glass vial overnight for the metal ion incorporation. The fabricated sensors were dried at room temperature under a house vacuum in a desiccator.

Chemiresistive Gas Sensing Measurements. The chemiresistive device was enclosed in a homemade Teflon gas flow chamber. The resistance of the device was measured over time (1 scan/s), with typical procedures including 15 min equilibration time (for the baseline resistance to stabilize) followed by 5 min exposure to analyte and then 15 min of recovery. All presented data are given as the numerical average ($N \ge 4$) accompanied by the standard deviation. The limit of detection was determined following reported procedures. 62-64

Wireless Device (*p*-CARD) **Preparation.** One mL portion of polymer/SWCNT dispersion was added with 1 mg of copper(I) triflate toluene complex, diluted with 4 mL of oDCB, and bath sonicated for 30 min. Two drops (0.5 μ L each) of the resulting dispersion were drop-casted onto the commercial RFID tag in locations following previously reported procedures 43,72,78 to convert the RFID tag to a p-CARD. After drop-casting, the p-CARDs were dried at room temperature under house vacuum in a desiccator.

Device RF Response Characterization. According to reported procedures, 43,72,78 p-CARDs were placed in a house-made sensing chamber connected to gas flow. The RF signal responses of p-CARDs

were measured from $10-20~\mathrm{MHz}$ with a custom-made loop probe connected via a BNC cable to a vector network analyzer (VNA) (Agilent ES061B). The distance between the probe and the device in the sensing enclosure was fixed throughout an experiment. The minimum gain value at the resonance frequency (in dB) was measured and acquired. The typical procedures include 15 min of equilibration time (for the baseline resistance to stabilize) followed by 15 min of exposure to analyte and then 60 min of recovery.

ASSOCIATED CONTENT

Supporting Information

The Supporting Information is available free of charge at https://pubs.acs.org/doi/10.1021/acsnano.3c07325.

Additional sensing and characterization data (XPS, Raman. NMR spectra) (PDF)

AUTHOR INFORMATION

Corresponding Author

Timothy M. Swager — Department of Chemistry and Institute for Soldier Nanotechnologies, Massachusetts Institute of Technology, Cambridge, Massachusetts 02139, United States; orcid.org/0000-0002-3577-0510; Email: tswager@mit.edu

Author

Shao-Xiong Lennon Luo — Department of Chemistry and Institute for Soldier Nanotechnologies, Massachusetts Institute of Technology, Cambridge, Massachusetts 02139, United States; orcid.org/0000-0001-5308-4576

Complete contact information is available at: https://pubs.acs.org/10.1021/acsnano.3c07325

Notes

The authors declare no competing financial interest.

ACKNOWLEDGMENTS

The authors gratefully acknowledge National Science Foundation (DMR-2207299). This work was performed in part at the Harvard University Center for Nanoscale Systems (CNS); a member of the National Nanotechnology Coordinated Infrastructure Network (NNCI), which is supported by the National Science Foundation under NSF award no. ECCS-2025158.

REFERENCES

- (1) Romagnani, P.; Remuzzi, G.; Glassock, R.; Levin, A.; Jager, K. J.; Tonelli, M.; Massy, Z.; Wanner, C.; Anders, H.-J. Chronic Kidney Disease. *Nat. Rev. Dis. Primers* **2017**, *3*, 17088.
- (2) Kalantar-Zadeh, K.; Jafar, T. H.; Nitsch, D.; Neuen, B. L.; Perkovic, V. Chronic Kidney Disease. *Lancet* **2021**, 398, 786–802.
- (3) Jha, V.; Garcia-Garcia, G.; Iseki, K.; Li, Z.; Naicker, S.; Plattner, B.; Saran, R.; Wang, A. Y.-M.; Yang, C.-W. Chronic Kidney Disease: Global Dimension and Perspectives. *Lancet* **2013**, 382, 260–272.
- (4) Levey, A. S.; Eckardt, K.-U.; Tsukamoto, Y.; Levin, A.; Coresh, J.; Rossert, J.; Zeeuw, D. D. E.; Hostetter, T. H.; Lameire, N.; Eknoyan, G. Definition and Classification of Chronic Kidney Disease: A Position Statement from Kidney Disease: Improving Global Outcomes (KDIGO). *Kidney Int.* 2005, 67, 2089–2100.
- (5) Levey, A. S.; Coresh, J.; Balk, E.; Kausz, A. T.; Levin, A.; Steffes, M. W.; Hogg, R. J.; Perrone, R. D.; Lau, J.; Eknoyan, G. National Kidney Foundation Practice Guidelines for Chronic Kidney Disease: Evaluation, Classification, and Stratification. *Ann. Int. Med.* **2003**, *139*, 137–147.

- (6) Barsoum, R. S. Chronic Kidney Disease in the Developing World. N. Engl. J. Med. 2006, 354, 997–999.
- (7) Testing and Treatment: Find It Early, Treat It Early. 2022. https://www.cdc.gov/kidneydisease/publications-resources/annual-report/ckd-testing-treatment.html (accessed May 1, 2023).
- (8) Seow, Y.-Y.; Cheung, Y. B.; Qu, L. M.; Yee, A. C. P. Trajectory of Quality of Life for Poor Prognosis Stage 5D Chronic Kidney Disease with and without Dialysis. *Am. J. Nephrol.* **2013**, *37*, 231–238.
- (9) Nickolas, T. L.; Frisch, G. D.; Opotowsky, A. R.; Arons, R.; Radhakrishnan, J. Awareness of Kidney Disease in the Us Population: Findings from the National Health and Nutrition Examination Survey (NHANES) 1999 to 2000. *Am. J. Kidney Dis.* **2004**, *44*, 185–197.
- (10) Vassalotti, J. A.; Stevens, L. A.; Levey, A. S. Testing for Chronic Kidney Disease: A Position Statement from the National Kidney Foundation. *Am. J. Kidney Dis.* **2007**, *50*, 169–180.
- (11) Chan, M.-J.; Li, Y.-J.; Wu, C.-C.; Lee, Y.-C.; Zan, H.-W.; Meng, H.-F.; Hsieh, M.-H.; Lai, C.-S.; Tian, Y.-C. Breath Ammonia Is a Useful Biomarker Predicting Kidney Function in Chronic Kidney Disease Patients. *Biomedicines* **2020**, *8*, 468.
- (12) Davies, S.; Spanel, P.; Smith, D. Quantitative Analysis of Ammonia on the Breath of Patients in End-Stage Renal Failure. *Kidney Int.* **1997**, 52, 223–228.
- (13) Rolla, G.; Bruno, M.; Bommarito, L.; Heffler, E.; Ferrero, N.; Petrarulo, M.; Bagnis, C.; Bugiani, M.; Guida, G. Breath Analysis in Patients with End-Stage Renal Disease: Effect of Haemodialysis. *Eur. J. Clin. Investig.* **2008**, 38, 728–733.
- (14) Ricci, P. P.; Gregory, O. J. Sensors for the Detection of Ammonia as a Potential Biomarker for Health Screening. *Sci. Rep.* **2021**, *11*, 7185.
- (15) Hibbard, T.; Killard, A. J. Breath Ammonia Levels in a Normal Human Population Study as Determined by Photoacoustic Laser Spectroscopy. *J. Breath Res.* **2011**, *5*, No. 037101.
- (16) Tsujii, M.; Kawano, S.; Tsuji, S.; Fusamoto, H.; Kamada, T.; Sato, N. Mechanism of Gastric Mucosal Damage Induced by Ammonia. *Gastroenterology* **1992**, *102*, 1881–1888.
- (17) Kearney, D. J.; Hubbard, T.; Putnam, D. Breath Ammonia Measurement in *Helicobacter Pylori* Infection. *Dig. Dis. Sci.* **2002**, *47*, 2523–2530.
- (18) Chittajallu, R. S.; Neithercut, W. D.; Macdonald, A. M.; McColl, K. E. Effect of Increasing *Helicobacter Pylori* Ammonia Production by Urea Infusion on Plasma Gastrin Concentrations. *Gut* 1991, 32, 21.
- (19) Gordon, N. Ornithine Transcarbamylase Deficiency: A Urea Cycle Defect. Eur. J. Paediatr. Neurol. 2003, 7, 115–121.
- (20) Torkzaban, M.; Haddad, A.; Baxter, J. K.; Berghella, V.; Gahl, W. A.; Al-Kouatly, H. B. Maternal Ornithine Transcarbamylase Deficiency, a Genetic Condition Associated with High Maternal and Neonatal Mortality Every Clinician Should Know: A Systematic Review. Am. J. Med. Genet. A 2019, 179, 2091–2100.
- (21) Wraith, J. E. Ornithine Carbamoyltransferase Deficiency. *Arch. Dis. Child.* **2001**, *84*, 84.
- (22) Grabowska-Polanowska, B.; Faber, J.; Skowron, M.; Miarka, P.; Pietrzycka, A.; Śliwka, I.; Amann, A. Detection of Potential Chronic Kidney Disease Markers in Breath Using Gas Chromatography with Mass-Spectral Detection Coupled with Thermal Desorption Method. *J. Chromatogr. A* **2013**, *1301*, 179–189.
- (23) Neri, G.; Lacquaniti, A.; Rizzo, G.; Donato, N.; Latino, M.; Buemi, M. Real-Time Monitoring of Breath Ammonia During Haemodialysis: Use of Ion Mobility Spectrometry (IMS) and Cavity Ring-Down Spectroscopy (CRDS) Techniques. *Nephrol. Dial. Transplant.* **2012**, *27*, 2945–2952.
- (24) Jazan, E.; Mirzaei, H. Direct Analysis of Human Breath Ammonia Using Corona Discharge Ion Mobility Spectrometry. *J. Pharm. Biomed. Anal.* **2014**, *88*, 315–320.
- (25) Wang, J.; Zhang, W.; Li, L.; Yu, Q. Breath Ammonia Detection Based on Tunable Fiber Laser Photoacoustic Spectroscopy. *Appl. Phys. B: Laser Opt.* **2011**, *103*, 263–269.
- (26) Buckley, S. G.; Damm, C. J.; Vitovec, W. M.; Sgro, L. A.; Sawyer, R. F.; Koshland, C. P.; Lucas, D. Ammonia Detection and

- Monitoring with Photofragmentation Fluorescence. Appl. Opt. 1998, 37, 8382–8391.
- (27) Heidt, B.; Siqueira, W. F.; Eersels, K.; Diliën, H.; van Grinsven, B.; Fujiwara, R. T.; Cleij, T. J. Point of Care Diagnostics in Resource-Limited Settings: A Review of the Present and Future of Poc in Its Most Needed Environment. *Biosensors* **2020**, *10*, 133.
- (28) Srinivasan, P.; Ezhilan, M.; Kulandaisamy, A. J.; Babu, K. J.; Rayappan, J. B. B. Room Temperature Chemiresistive Gas Sensors: Challenges and Strategies—a Mini Review. *J. Mater. Sci.: Mater. Electron* **2019**, *30*, 15825–15847.
- (29) Ramgir, N.; Datta, N.; Kaur, M.; Kailasaganapathi, S.; Debnath, A. K.; Aswal, D. K.; Gupta, S. K. Metal Oxide Nanowires for Chemiresistive Gas Sensors: Issues, Challenges and Prospects. *Colloids Surf., A* **2013**, 439, 101–116.
- (30) Fratoddi, I.; Venditti, I.; Cametti, C.; Russo, M. V. Chemiresistive Polyaniline-Based Gas Sensors: A Mini Review. *Sens. Actuators B Chem.* **2015**, 220, 534–548.
- (31) Koo, W.-T.; Jang, J.-S.; Kim, I.-D. Metal-Organic Frameworks for Chemiresistive Sensors. *Chem* **2019**, *5*, 1938–1963.
- (32) Schroeder, V.; Savagatrup, S.; He, M.; Lin, S.; Swager, T. M. Carbon Nanotube Chemical Sensors. *Chem. Rev.* **2019**, *119*, 599–663.
- (33) Luo, S.-X. L.; Swager, T. M. Chemiresistive Sensing with Functionalized Carbon Nanotubes. *Nat. Rev. Methods Primers* **2023**, 3, 73
- (34) Norizan, M. N.; Moklis, M. H.; Ngah Demon, S. Z.; Halim, N. A.; Samsuri, A.; Mohamad, I. S.; Knight, V. F.; Abdullah, N. Carbon Nanotubes: Functionalisation and Their Application in Chemical Sensors. *RSC Adv.* **2020**, *10*, 43704–43732.
- (35) Chen, K.; Gao, W.; Emaminejad, S.; Kiriya, D.; Ota, H.; Nyein, H. Y. Y.; Takei, K.; Javey, A. Printed Carbon Nanotube Electronics and Sensor Systems. *Adv. Mater.* **2016**, *28*, 4397–4414.
- (36) Ellis, J. E.; Star, A. Carbon Nanotube Based Gas Sensors toward Breath Analysis. *ChemPlusChem.* **2016**, *81*, 1248–1265.
- (37) Xiang, L.; Zhang, H.; Hu, Y.; Peng, L.-M. Carbon Nanotube-Based Flexible Electronics. J. Mater. Chem. C 2018, 6, 7714–7727.
- (38) Kumar, S.; Pavelyev, V.; Mishra, P.; Tripathi, N. A Review on Chemiresistive Gas Sensors Based on Carbon Nanotubes: Device and Technology Transformation. *Sens. Actuator A Phys.* **2018**, 283, 174–186.
- (39) Luo, S.-X. L.; Lin, C.-J.; Ku, K. H.; Yoshinaga, K.; Swager, T. M. Pentiptycene Polymer/Single-Walled Carbon Nanotube Complexes: Applications in Benzene, Toluene, and O-Xylene Detection. *ACS Nano* **2020**, *14*, 7297–7307.
- (40) Luo, S.-X. L.; Yuan, W.; Xue, M.; Feng, H.; Bezdek, M. J.; Palacios, T.; Swager, T. M. Chemiresistive Hydrogen Sensing with Size-Limited Palladium Nanoparticles in Iptycene-Containing Poly-(Arylene Ether)S. ACS Nano 2023, 17, 2679–2688.
- (41) Yoon, B.; Liu, S. F.; Swager, T. M. Surface-Anchored Poly(4-Vinylpyridine)—Single-Walled Carbon Nanotube—Metal Composites for Gas Detection. *Chem. Mater.* **2016**, 28, 5916—5924.
- (42) Koo, W.-T.; Kim, Y.; Savagatrup, S.; Yoon, B.; Jeon, I.; Choi, S.-J.; Kim, I.-D.; Swager, T. M. Porous Ion Exchange Polymer Matrix for Ultrasmall Au Nanoparticle-Decorated Carbon Nanotube Chemiresistors. *Chem. Mater.* **2019**, *31*, 5413–5420.
- (43) Zhu, R.; Desroches, M.; Yoon, B.; Swager, T. M. Wireless Oxygen Sensors Enabled by Fe(II)-Polymer Wrapped Carbon Nanotubes. *ACS Sens.* **2017**, *2*, 1044–1050.
- (44) Ishihara, S.; O'Kelly, C. J.; Tanaka, T.; Kataura, H.; Labuta, J.; Shingaya, Y.; Nakayama, T.; Ohsawa, T.; Nakanishi, T.; Swager, T. M. Metallic Versus Semiconducting SWCNT Chemiresistors: A Case for Separated Swcnts Wrapped by a Metallosupramolecular Polymer. ACS Appl. Mater. Interfaces 2017, 9, 38062–38067.
- (45) Jorio, A; Pimenta, M A; Filho, A G S.; Saito, R; Dresselhaus, G; Dresselhaus, M S Characterizing Carbon Nanotube Samples with Resonance Raman Scattering. *New J. Phys.* **2003**, *5*, 139.
- (46) Dresselhaus, M. S.; Dresselhaus, G.; Jorio, A.; Souza Filho, A. G.; Saito, R. Raman Spectroscopy on Isolated Single Wall Carbon Nanotubes. *Carbon* **2002**, *40*, 2043–2061.

- (47) Yoshida, T. An X-Ray Photoelectron Spectroscopic Study of Several Ligands in Coordination Compounds. *Bull. Chem. Soc. Jpn.* **1980**, 53, 1327–1330.
- (48) Zakharova, I. A.; Salyn, J. V.; Tatjanenko, L. V.; Mashkovsky, Y. S.; Ponticelli, G. Inhibitory Activity of Palladium(II) and Platinum(II) Complexes with Isoxazole and Its Derivatives. *J. Inorg. Biochem.* **1981**, 15, 89–92.
- (49) Luo, S.-X. L.; Liu, R. Y.; Lee, S.; Swager, T. M. Electrocatalytic Isoxazoline—Nanocarbon Metal Complexes. *J. Am. Chem. Soc.* **2021**, 143, 10441—10453.
- (50) Biesinger, M. C. Advanced Analysis of Copper X-Ray Photoelectron Spectra. Surf. Interface Anal. 2017, 49, 1325–1334.
- (51) Ozawa, H.; Ide, N.; Fujigaya, T.; Niidome, Y.; Nakashima, N. One-Pot Separation of Highly Enriched (6,5)-Single-Walled Carbon Nanotubes Using a Fluorene-Based Copolymer. *Chem. Lett.* **2011**, *40*, 239–241.
- (52) Graf, A.; Zakharko, Y.; Schießl, S. P.; Backes, C.; Pfohl, M.; Flavel, B. S.; Zaumseil, J. Large Scale, Selective Dispersion of Long Single-Walled Carbon Nanotubes with High Photoluminescence Quantum Yield by Shear Force Mixing. *Carbon* **2016**, *105*, 593–599.
- (53) Joo, Y.; Brady, G. J.; Shea, M. J.; Oviedo, M. B.; Kanimozhi, C.; Schmitt, S. K.; Wong, B. M.; Arnold, M. S.; Gopalan, P. Isolation of Pristine Electronics Grade Semiconducting Carbon Nanotubes by Switching the Rigidity of the Wrapping Polymer Backbone on Demand. ACS Nano 2015, 9, 10203–10213.
- (54) Peveler, W. J.; Yazdani, M.; Rotello, V. M. Selectivity and Specificity: Pros and Cons in Sensing. ACS Sens. 2016, 1, 1282–1285.
- (55) Rath, R. J.; Farajikhah, S.; Oveissi, F.; Dehghani, F.; Naficy, S. Chemiresistive Sensor Arrays for Gas/Volatile Organic Compounds Monitoring: A Review. *Adv. Eng. Mater.* **2023**, *25*, No. 2200830.
- (56) Moon, H. G.; Jung, Y.; Han, S. D.; Shim, Y.-S.; Shin, B.; Lee, T.; Kim, J.-S.; Lee, S.; Jun, S. C.; Park, H.-H.; et al. Chemiresistive Electronic Nose toward Detection of Biomarkers in Exhaled Breath. ACS Appl. Mater. Interfaces 2016, 8, 20969–20976.
- (57) Quang, N. H.; Van Trinh, M.; Lee, B.-H.; Huh, J.-S. Effect of NH3 Gas on the Electrical Properties of Single-Walled Carbon Nanotube Bundles. *Sens. Actuators B Chem.* **2006**, *113*, 341–346.
- (58) Goldoni, A.; Larciprete, R.; Petaccia, L.; Lizzit, S. Single-Wall Carbon Nanotube Interaction with Gases: Sample Contaminants and Environmental Monitoring. *J. Am. Chem. Soc.* **2003**, *125*, 11329–11333.
- (59) Liu, S. F.; Petty, A. R.; Sazama, G. T.; Swager, T. M. Single-Walled Carbon Nanotube/Metalloporphyrin Composites for the Chemiresistive Detection of Amines and Meat Spoilage. *Angew. Chem., Int. Ed.* **2015**, *54*, 6554–6557.
- (60) Liang, X.; Chen, Z.; Wu, H.; Guo, L.; He, C.; Wang, B.; Wu, Y. Enhanced NH₃-Sensing Behavior of 2,9,16,23-Tetrakis(2,2,3,3-Tetrafluoropropoxy) Metal(II) Phthalocyanine/Multi-Walled Carbon Nanotube Hybrids: An Investigation of the Effects of Central Metals. *Carbon* **2014**, *80*, 268–278.
- (61) Kaya, E. N.; Basova, T.; Polyakov, M.; Durmuş, M.; Kadem, B.; Hassan, A. Hybrid Materials of Pyrene Substituted Phthalocyanines with Single-Walled Carbon Nanotubes: Structure and Sensing Properties. *RSC Adv.* **2015**, *5*, 91855–91862.
- (62) Fong, D.; Luo, S.-X. L.; Andre, R. S.; Swager, T. M. Trace Ethylene Sensing Via Wacker Oxidation. *ACS Cent. Sci.* **2020**, *6*, 507–512.
- (63) Mirica, K. A.; Weis, J. G.; Schnorr, J. M.; Esser, B.; Swager, T. M. Mechanical Drawing of Gas Sensors on Paper. *Angew. Chem., Int. Ed.* **2012**, *51*, 10740–10745.
- (64) Li, J.; Lu, Y.; Ye, Q.; Cinke, M.; Han, J.; Meyyappan, M. Carbon Nanotube Sensors for Gas and Organic Vapor Detection. *Nano Lett.* **2003**, *3*, 929–933.
- (65) Morselli-Labate, A. M.; Fantini, L.; Pezzilli, R. Hydrogen Sulfide, Nitric Oxide and a Molecular Mass 66u Substance in the Exhaled Breath of Chronic Pancreatitis Patients. *Pancreatology* **2007**, 7, 497–504.

- (66) Birg, A.; Hu, S.; Lin, H. C. Reevaluating Our Understanding of Lactulose Breath Tests by Incorporating Hydrogen Sulfide Measurements. *IGH Open* **2019**, *3*, 228–233.
- (67) Prabhakar, A.; Iglesias, R. A.; Shan, X.; Xian, X.; Zhang, L.; Tsow, F.; Forzani, E. S.; Tao, N. Online Sample Conditioning for Portable Breath Analyzers. *Anal. Chem.* **2012**, *84*, 7172–7178.
- (68) Romero, H. E.; Sumanasekera, G. U.; Kishore, S.; Eklund, P. C. Effects of Adsorption of Alcohol and Water on the Electrical Transport of Carbon Nanotube Bundles. *J. Phys.: Condens. Matter* **2004**, *16*, 1939.
- (69) Na, P. S.; Kim, H.; So, H.-M.; Kong, K.-J.; Chang, H.; Ryu, B. H.; Choi, Y.; Lee, J.-O; Kim, B.-K.; Kim, J.-J.; Kim, J.; et al. Investigation of the Humidity Effect on the Electrical Properties of Single-Walled Carbon Nanotube Transistors. *Appl. Phys. Lett.* **2005**, 87, No. 093101.
- (70) Randeniya, L. K.; Martin, P. J. Removal of Strongly-Bound Gases from Single-Walled Carbon Nanotubes without Annealing or Ultraviolet Light Exposure. *Carbon* **2013**, *60*, 498–505.
- (71) Azzarelli, J. M.; Mirica, K. A.; Ravnsbæk, J. B.; Swager, T. M. Wireless Gas Detection with a Smartphone Via RF Communication. *Proc. Natl. Acad. Sci. U. S. A.* **2014**, *111*, 18162–18166.
- (72) Zhu, R.; Azzarelli, J. M.; Swager, T. M. Wireless Hazard Badges to Detect Nerve-Agent Simulants. *Angew. Chem., Int. Ed.* **2016**, *55*, 9662–9666
- (73) Li, J.; Yuan, W.; Luo, S.-X. L.; Bezdek, M. J.; Peraire-Bueno, A.; Swager, T. M. Wireless Lateral Flow Device for Biosensing. *J. Am. Chem. Soc.* **2022**, *144*, 15786–15792.
- (74) Jing, H. C.; Wang, Y. E. Capacity Performance of an Inductively Coupled near Field Communication System. *IEEE Antennas and Propagation Society International Symposium*; San Diego, CA, July 5–11, 2008; pp 1–4. DOI: 10.1109/APS.2008.4619268.
- (75) Yang, J.-S.; Swager, T. M. Fluorescent Porous Polymer Films as TNT Chemosensors: Electronic and Structural Effects. *J. Am. Chem. Soc.* **1998**, *120*, 11864–11873.
- (76) Lee, J.; Malekshahi Byranvand, M.; Kang, G.; Son, S. Y.; Song, S.; Kim, G.-W.; Park, T. Green-Solvent-Processable, Dopant-Free Hole-Transporting Materials for Robust and Efficient Perovskite Solar Cells. J. Am. Chem. Soc. 2017, 139, 12175–12181.
- (77) Bouffard, J.; Swager, T. M. Fluorescent Conjugated Polymers That Incorporate Substituted 2,1,3-Benzooxadiazole and 2,1,3-Benzothiadiazole Units. *Macromolecules* **2008**, *41*, 5559–5562.
- (78) Andre, R. S.; Ngo, Q. P.; Fugikawa-Santos, L.; Correa, D. S.; Swager, T. M. Wireless Tags with Hybrid Nanomaterials for Volatile Amine Detection. *ACS Sens.* **2021**, *6*, 2457–2464.